ACES Asian Chemical Editorial Society

doi.org/10.1002/ajoc.202500372

ASIAN JOURNAL OF ORGANIC CHEMISTRY
Research Article

www.asianjoc.org

Tuning Antiaromaticity Through *Meso*-Substituent Orientation in Core-Modified Isophlorins

Maika Isoda,[a] Haruna Sugimura,[a] Yusuke Honda,[a] and Ken-ichi Yamashita*[a, b]

Dedicated to the memory of Professor Masahiko Iyoda

Antiaromaticity is an essential principle in organic chemistry that significantly influences the properties of cyclic π-conjugated systems. This study systematically investigated the effects of *meso*-substituents on the antiaromaticity of dithiadioxaisophlorins (S_2O_2Iphs), which are stable isophlorin derivatives with strong antiaromatic characteristics. We synthesized two new S_2O_2Iphs derivatives with 3,5-bis(trifluoromethyl)phenyl and 5-cyanothien-2-yl substituents along with a previously reported pentafluorophenyl-substituted analog. Notably, a derivative with sterically demanding 2,6-dichlorophenyl substituents could not be isolated despite being detected by mass spectrometry, highlighting the delicate balance between electronic stabilization, and steric effects. Through comprehensive analysis using ^{1}H NMR spectroscopy, UV/vis absorption spectroscopy, and multiple computational approaches (NICS, GIMIC, HOMA/HOMAc, and AV1245/AV_{min}), we demonstrate that the steric bulkiness of *meso*-substituents predominantly determines their tilt angle relative to the isophlorin macrocycle, critically influencing antiaromaticity. Bulkier substituents maintain larger tilt angles, preserving stronger antiaromaticity, while less bulky groups allow greater π-conjugation with the macrocycle, thereby reducing antiaromaticity. These findings provide valuable guidance for the design of functional antiaromatic materials with tunable electronic properties.

1. Introduction

Aromaticity and antiaromaticity are fundamental concepts in organic chemistry that significantly influence the properties of cyclic π-conjugated systems.[1–3] While aromatic compounds following Hückel's $(4n+2)\pi$-electron rule are well-studied due to their stability, antiaromatic compounds with $4n\pi$-electrons remain rare due to their inherent instability. However, understanding antiaromaticity is crucial not only for fundamental chemistry, but also because antiaromatic compounds exhibit unique electronic properties that make them promising candidates for organic electronic materials and optoelectronic devices.[4–13]

Recent advances in synthesis have enabled the preparation of increasingly stable antiaromatic systems, renewing interest in their properties, and applications. Among these, porphyrinoid-based antiaromatic molecules,[14–16] particularly isophlorins (two electron-reduced porphyrins),[17,18] have emerged as valuable platforms for investigating antiaromaticity. Core-modified isophlorins, where heteroatoms, such as oxygen and sulfur replace pyrrole nitrogen atoms, offer opportunities to modulate their electronic structure and stability.[19,20]

The properties of antiaromatic compounds can be tuned through various structural modifications. Recent studies have revealed that substituents influence their electronic structure, stability, and assembly behavior. Among antiaromatic porphyrinoids, norcorrole derivatives are extensively studied with various aryl and alkyl substituents at *meso*-positions.[21–30] However, the relationship between substituent effects and antiaromaticity has not yet been systematically discussed in these compounds.

Several studies have provided important insights into substituent effects on antiaromatic systems. Takase and coworkers demonstrated that the electronic properties of π-extended antiaromatic systems can be systematically controlled by altering the structural relationship between substituents and the macrocycle.[31] Salikov and coworkers showed that the antiaromaticity of cycloheptatrienyl anions is primarily determined by the geometry of the anion, which in turn is controlled by the substituent properties.[32] More recently, Shimizu and coworkers reported that *meso*-substituents of 5,15-dioxaporphyrins affect their crystal packing and oxidation behavior, although the antiaromaticity itself was relatively unchanged in their system.[33]

[a] *M. Isoda, H. Sugimura, Y. Honda, Dr. K.-ichi Yamashita*
Department of Chemistry, Graduate School of Science, The University of Osaka, 1-1 Machikaneyama, Toyonaka, Osaka 560-0043, Japan
E-mail: yamashita-k@chem.sci.osaka-u.ac.jp

[b] *Dr. K.-ichi Yamashita*
Innovative Catalysis Science Division, Institute for Open and Transdisciplinary Research Initiatives (ICS-OTRI), The University of Osaka, Suita, Osaka 565–0871, Japan

Maika Isoda and Haruna Sugimura have contributed equally to this work.

Supporting information for this article is available on the WWW under https://doi.org/10.1002/ajoc.202500372

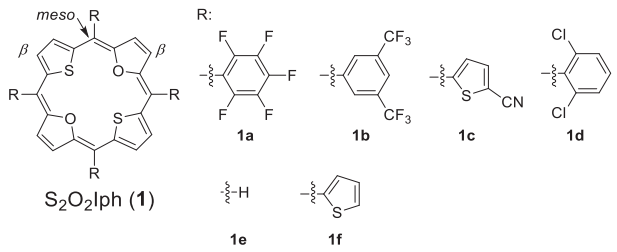

Figure 1. Structure of S_2O_2Iphs (**1**).

Our previous work demonstrated that introducing electron-withdrawing cyano groups at the β-positions of isophlorins significantly enhanced their stability while reducing antiaromaticity due to π-conjugation effects.[34,35] These studies suggest that the relationship between substituents and antiaromaticity vary significantly depending on the molecular framework and position of substitution.

Herein, we report a systematic investigation of the effects of *meso*-substituents on dithiadioxaisophlorins (S_2O_2Iphs, **1**; Figure 1), which are attainable stable isophlorin derivatives with strong antiaromatic characteristics.[17,18,20] While pentafluorophenyl-substituted S_2O_2Iph (**1a**) was reported by Anand and coworkers,[20] we synthesized two new derivatives with 3,5-bis(trifluoromethyl)phenyl (**1b**) and 5-cyanothien-2-yl (**1c**) substituents. Combining experimental techniques and computational methods, we investigated how different *meso*-substituents influence the electronic properties of these compounds, focusing on the interplay between steric demands and electronic effects in controlling antiaromaticity.

2. Results and Discussion

2.1. Synthesis

Isophlorins are generally unstable toward oxidation because of their antiaromatic character and high-energy HOMO levels.[17–19] Previous studies have indicated that electron-withdrawing substituents at the *meso*-positions are crucial for stabilizing these compounds.[20] Therefore, we synthesized four S_2O_2Iphs (**1a–d**) with varying steric properties of the electron-withdrawing *meso*-substituents to systematically investigate their effects on antiaromaticity and stability.

Compounds **1a–d** were synthesized following a modified procedure from **2a–d** reported by Anand and coworkers (Scheme 1).[20] The previously reported pentafluorophenyl-substituted derivative **1a** was successfully synthesized and isolated.[20] A 7% yield of the new derivative **1b,** with 3,5-bis(trifluoromethyl)phenyl groups, was obtained by synthesizing similarly to **1a**.

For **1c** bearing 5-cyanothien-2-yl substituents, direct cyclization produced a mixture of the desired product with an S_3O_3hexaphyrin analog (Figure S1),[36] which proved difficult to separate using conventional silica gel column chromatography. Therefore, an alternative two-step synthetic route involving intermediate **3c** was developed to obtain **1c**.

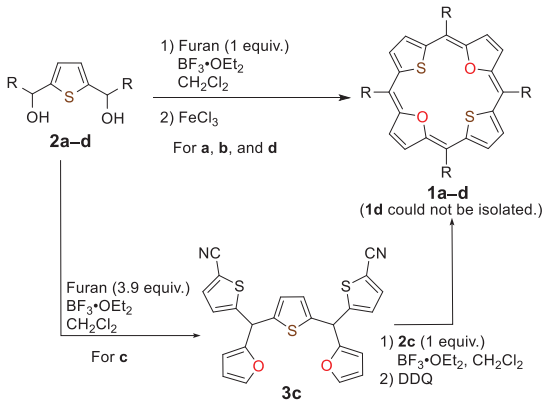

Scheme 1. Synthetic route to S_2O_2Iphs **1a**, **1b**, **1c**, and **1d**.

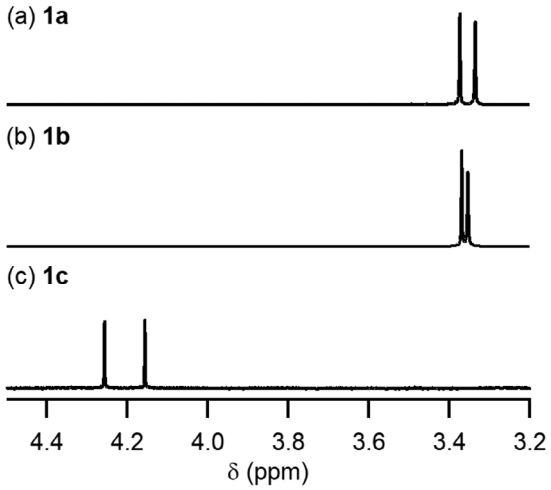

Figure 2. ^{1}H NMR ($CDCl_3$, rt) spectra showing two β proton signals of S_2O_2Iph. (a) **1a** (500 MHz), (b) **1b** (400 MHz), and (c) **1c** (400 MHz).

For **1d** with 2,6-dichlorophenyl substituents, although mass spectrometric analysis of the crude product showed the expected molecular ion peak by mass spectrometry (Figure S2a), attempts to isolate the pure compound were unsuccessful. The ^{1}H NMR spectrum showed no distinct signals (Figure S2b), suggesting rapid aerobic oxidation or decomposition under ambient conditions.

2.2. Evaluation of Antiaromaticity by ^{1}H NMR Spectroscopy

The antiaromatic character of the synthesized S_2O_2Iphs was evaluated using ^{1}H NMR spectroscopy (Figure 2). The β-protons of both **1a** and **1b** exhibited characteristic upfield-shifted singlets at approximately 3.35 ppm, indicating strong paratropic ring currents and pronounced antiaromaticity. In contrast, the corresponding signals for **1c** appeared at 4.26 and 4.16 ppm, which were significantly downfield-shifted compared to those of **1a** and **1b**. This suggests a weaker paratropic ring current, indicating diminished antiaromaticity in **1c** relative to **1a** and **1b**. Another likely contributing factor is the varying degrees of the shielding effects of the aromatic substituents.[33] Therefore, we conducted a comprehensive investigation using various antiaromaticity indices to fully evaluate these effects.

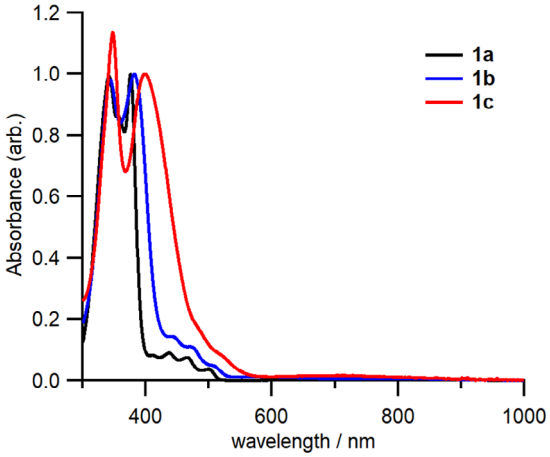

Figure 3. UV/vis absorption spectra of **1a**, **1b**, and **1c** in CH_2Cl_2.

2.3. UV/vis Absorption Properties

The UV/vis absorption spectra of **1a**, **1b**, and **1c** in CH_2Cl_2 are shown in Figure 3. All compounds exhibited absorption patterns typical of antiaromatic porphyrinoids, with significant differences reflecting the varying degrees of antiaromaticity.

Each spectrum shows three main regions: (i) an intense absorption band within 380–420 nm, (ii) a series of moderately intense bands with a vibronic structure within 400–550 nm, and (iii) a very weak and broad absorption extending into the 600–1000 nm range. This long-wavelength absorption is attributed to the symmetry-forbidden HOMO–LUMO transition characteristic to antiaromatic compounds with narrow energy gaps. Notably, the spectral features of **1c** showed the most pronounced broadening and bathochromic shifts, followed by **1b**, whereas **1a** exhibited the sharpest and most blue-shifted absorption bands.

2.4. Theoretical Calculations—Structural Comparison

The geometry-optimized structures of S_2O_2Iphs (**1a**–**1c**) were obtained at the cam-B3LYP/6-311G(d,p) theory level in the gas phase, and are shown in Figure 4a–c exhibiting saddle-type distorted structures. Figure 4e–g shows the skeletal deviations of the macrocycle atoms from the mean plane defined by the 24 core atoms. The analysis revealed decreasing planarity (**1a** > **1b** > **1c**) with the thiophene rings showing larger deviations from the mean plane than the furan rings in all compounds. The mean plane deviation (mpd), which serves as an index of planarity, followed the order **1a** (0.223) < **1b** (0.303) < **1c** (0.354). The tilt angles between the *meso*-substituents and the mean plane of the isophlorin macrocycles decreased (**1a** (63.0°) > **1b** (52.1°) > **1c** (51.7°)) correlating with the steric bulkiness of the substituents and mpd values.

Notably, Valiev et al. also performed computational studies on compounds equivalent to **1a** and the *meso*-free analog **1e** in their investigation of the magnetically induced current pathways and optical properties of isophlorins.[37] However, their **1a** optimized structure exhibited imaginary frequencies related to the rotations of the C_6F_5 groups and was completely planar with the aryl groups positioned orthogonally to the isophlorin plane. In contrast, our **1a** optimized structure represents a true energy minimum without imaginary frequencies, suggesting that our calculated nonplanar saddle-shaped conformation is more reliable. To verify this, we performed geometry optimizations of four conformers of **1a** at the same computational level, including our reported saddle conformer (C_{2v}) and the completely planar

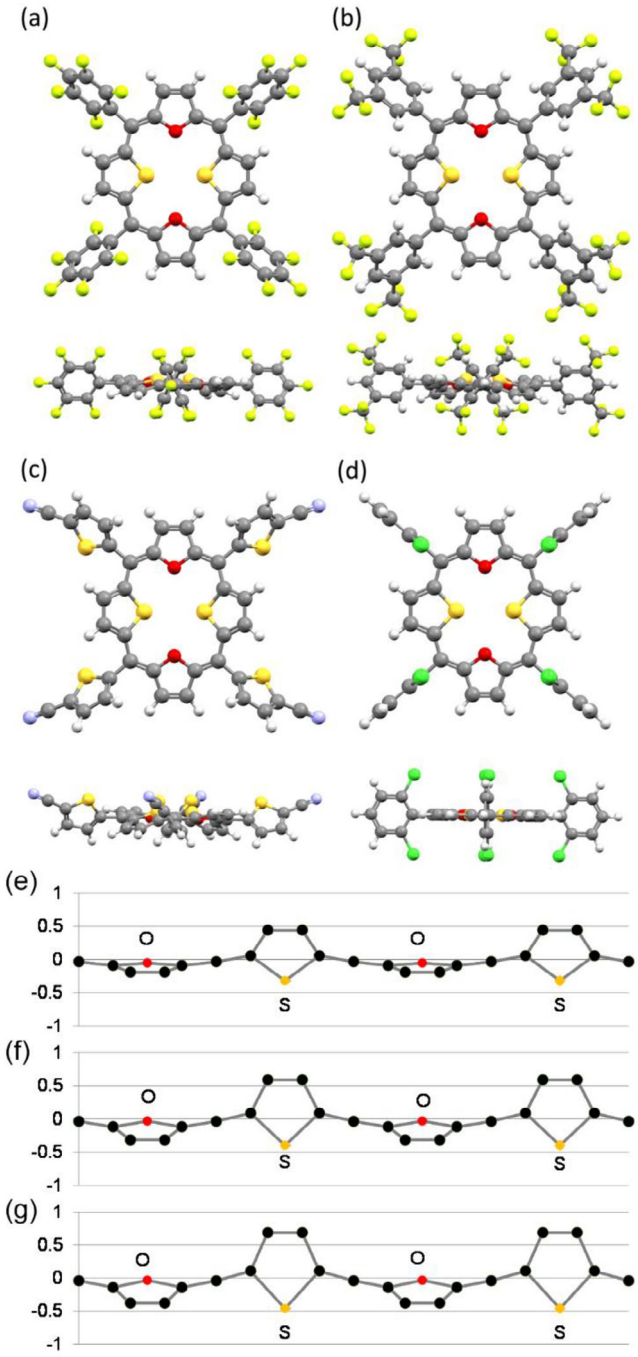

Figure 4. Information for geometry optimized structures. Top and side views of (a) **1a**, (b) **1b**, (c) **1c**, and (d) **1d**. Skeletal deviations (Å) of the macrocycle atoms from the 24-plane for the geometry-optimized structures of (e) **1a**, (f) **1b**, and (g) **1c**.

(D_{2h}) conformer, similar to the model of Valiev et al. An energy comparison confirmed that our saddle structure was more stable (Figure S9). The energy difference between this structure and the planar conformer without imaginary frequencies (D_2) was remarkably small (0.58 kcal mol^{-1}).

It is worth noting that Anand and coworkers previously reported the crystal structure of **1a**, which showed a nearly planar macrocycle conformation with *meso*-C_6F_5 groups at tilt angles of 72.5°,[20] in contrast to our calculated saddle-shaped geometry. This phenomenon of crystal-induced planarization has been occasionally observed in other antiaromatic porphyrinoids[34,35] and can be attributed to crystal packing forces in the solid state. The small energy difference we calculated between the saddle and planar conformers (0.58 kcal mol^{-1}) explains why crystal packing forces can readily induce planarization.

To further investigate the effect of *meso*-substituents on planarity, we performed geometry optimizations of **1d** and its *meso*-free analog **1e**. **1d** and **1e** exhibited perfectly planar structures with zero mpd unlike **1a**–**1c**. This demonstrates that non-bulky aryl substituents at the *meso*-positions reduce the planarity of isophlorin thus decreasing their antiaromaticity. The degree of planarity depends on substituent bulkiness, with the sterically demanding 2,6-dichlorophenyl groups in **1d** adopting an orthogonal orientation relative to the isophlorin macrocycle, thus minimizing their effect on planarity. For the unsubstituted isophlorin (**1e**), both our calculations and those of Valiev et al.[37] showed a completely planar structure without imaginary frequencies.

To investigate the influence of the cyano groups on the thiophene rings introduced for the stabilization of isophlorin **1c**, we calculated the structure of derivative **1f** without cyano groups. The mpd of **1f** was 0.294, indicating higher planarity (lower mpd) than **1c**. Additionally, the tilt angle of the substituents was larger (57.6°) than that of **1c**. These results demonstrate that the cyano groups on the thiophene rings significantly affect the structure of the isophlorin ring.

2.5. Theoretical Calculations—Electronic Structure Analysis

The steric bulkiness of substituents significantly influences the tilt angle relative to the isophlorin plane. Smaller tilt angles enhance π-electron perturbation between the isophlorin and aryl substituents, potentially reducing antiaromaticity through contributions from nonaromatic resonance structures. Molecular orbital (MO) analysis revealed that **1c**, with its smaller tilt angle, exhibited delocalized molecular orbitals extending across the molecule with more extensive π-conjugation toward the *meso*-substituents (Figures 5, and S10–S14). In contrast, compounds with larger tilt angles showed more localized π-conjugation. This computationally predicted extension of π-conjugation in **1c** is further corroborated by the observed bathochromic shifts and spectral broadening in its absorption spectrum.

The MO energy diagrams of **1a**–**f** (Figure 6) show that the HOMO energies of **1d**–**f** were substantially higher than those

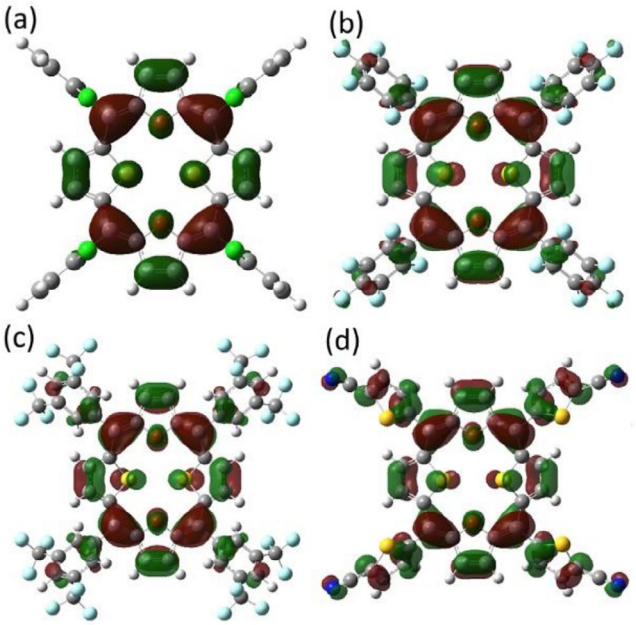

Figure 5. HOMO−1 of (a) **1d**, (b) **1a**, (c) **1b**, and (d) **1c**.

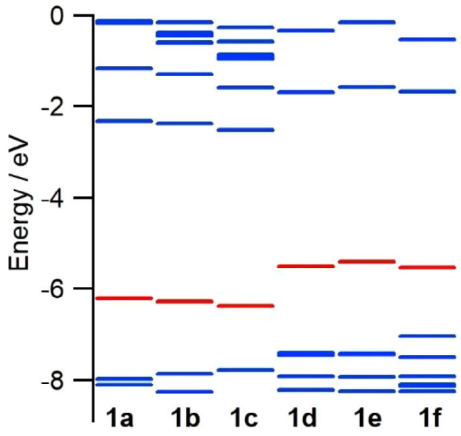

Figure 6. MO energy diagram of S_2O_2Iph **1**. The red lines highlight the HOMO energy level.

of the isolated compounds **1a**–**c**. This explains the instability of **1d**–**f** toward oxidation and highlights the importance of electron-withdrawing substituents in stabilizing isophlorins.

2.6. Evaluation of Antiaromaticity by Calculations

To quantitatively assess the antiaromaticity of S_2O_2Iphs, we employed multiple computational approaches based on magnetic, geometric, and electronic criteria.[3,38] These complementary methods provided a comprehensive understanding of the antiaromatic characteristics of our series of compounds (Table 1).

Nucleus-independent chemical shift (NICS)[39,40] calculations were performed based on the optimized structures at the center of the macrocycle. The NICS values, which measure the magnetic shielding at the center of the aromatic/antiaromatic ring (positive values indicating stronger antiaromaticity), revealed that the

Table 1. Antiaromatic indices for S_2O_2Iphs.

	$\delta(H_\beta)$[a]	NICS(0)[b]	NICS(1)[b]	GIMIC / nA T^{-1} [c]	mpd / Å	HOMA	HOMAc	AV1245	AV_{min}
1a	3.37, 3.33	11 (46)	11 (38)	16	0.223	0.433	0.676	1.12	0.80
1b	3.37, 3.35	9 (41)	9 (34)	14	0.303	0.426	0.673	1.12	0.74
1c	4.26, 4.16	8 (37)	8 (31)	12	0.354	0.430	0.676	1.10	0.72
1d	ND[d]	14 (56)	13 (44)	20	0	0.445	0.683	1.14	0.84
1e	ND[d]	16 (59)	14 (47)	21	0	0.473	0.698	1.25	0.92
1f	ND[d]	9 (41)	9 (35)	ND[d]	0.294	0.434	0.678	1.12	0.76

[a] ^{1}H NMR chemical shifts (ppm) for β protons ($CDCl_3$, rt, 500 MHz for **1a**, and 400 MHz for **1b** and **1c**). See Figure 2; [b] $NICS_{iso}$ values calculated at cam-B3LYP/6-311+G(2d,p)//cam-B3LYP/6-311G(d,p) Values in parentheses are $NICS_{zz}$ values; [c] Integrated current strengths passing through C_{meso}–C_α bonds; [d] No data.

antiaromaticity strength decreased (**1e** > **1d** > **1a** > **1b** ≈ **1f** > **1c**), correlating with the magnitude of the tilt angle between the *meso*-substituents and isophlorin macrocycles. Notably, **1d** and **1e** exhibited pronounced antiaromaticity, which is attributed to their completely planar isophlorin macrocycles.

To further validate these findings, the magnetically induced current densities were calculated using the program GIMIC.[41,42] The induced current density values followed the same trend as the NICS results: **1e** (21 nA T^{-1}) > **1d** (20 nA T^{-1}) > **1a** (16 nA T^{-1}) > **1b** (14 nA T^{-1}) > **1c** (12 nA T^{-1}), supporting our magnetic-based assessment of antiaromaticity. Notably, Valiev et al. also performed GIMIC calculations for compounds equivalent to **1a** and **1e** and reported a reduction in the paratropic ring current strength of **1a** compared to that of **1e**.[37,43] However, our calculations indicate a more pronounced decrease in antiaromaticity owing to the presence of *meso*-substituents. This difference is attributed to the aforementioned structural discrepancies.

To complement the magnetic criteria, we examined geometry-based aromatic/antiaromatic indices, including the harmonic oscillator model of aromaticity (HOMA)[44,45] and its improved version, HOMAc, considering both aromatic and antiaromatic compounds.[46] These indices provide insights into the bond length alternation patterns that are characteristic of aromatic and antiaromatic systems. For our calculations, we consistently defined the ring as encompassing all 24 carbon atoms of the isophlorin skeleton, as this was the most relevant conjugation pathway by comparison with other pathways (for **1e**, Figure S15) and localized orbital locator of π orbitals(LOL-π)[47] analysis (Figure S16), which visualized π-electron localization and delocalization within the molecule.

The HOMA values followed the order: **1e** (0.473) > **1d** (0.445) > **1f** (0.434) > **1a** (0.433) > **1c** (0.430) > **1b** (0.426). The HOMAc values were higher than the original HOMA values but maintained the same relative order. These geometric indices aligned with the magnetic indicators, with slight deviations in the relative positions of **1b** and **1c**. This minor discrepancy may reflect the influence of extended π-conjugation with substituents in **1c**, which affects bond length alternation patterns while having less impact on magnetic properties.

Finally, we evaluated electronic aromaticity indices,[38] specifically AV1245[48] and AV_{min},[49,50] which were developed for assessing antiaromaticity in large cyclic π-conjugated systems such as porphyrinoids.[50–52] Recent studies have suggested AV_{min} as the most reliable electronic indicator for antiaromaticity.[50,51] Both indices identified **1e** and **1c** as having the highest and lowest antiaromaticity, respectively, which is consistent with our conclusions based on other indicators. The AV_{min} values, in particular, showed perfect agreement with the order established by the NICS and GIMIC calculations. The AV1245 values were also in agreement, except for those of compounds **1a**, **1b**, and **1f**, which had similar values.

Based on this comprehensive analysis integrating experimental ^{1}H NMR data, structural planarity measurements, and multiple computational indicators (NICS, GIMIC, HOMA/HOMAc, and AV1245/AV_{min}), we determined that the antiaromatic character of these systems decreases in the order **1e** > **1d** > **1a** > **1b** (≈ **1f**) > **1c**. This trend consistently demonstrates the significant influence of *meso*-substituents on the antiaromaticity of isophlorins, primarily through their effect on macrocycle planarity and the extent of π-conjugation.

3. Conclusion

This study systematically investigated the effect of *meso*-substituents on the antiaromaticity of S_2O_2Iphs. Through a comprehensive analysis integrating experimental ^{1}H NMR data and multiple computational approaches (NICS, GIMIC, HOMA/HOMAc, and AV1245/AV_{min}), we demonstrated that the steric demands of *meso*-substituents critically influence antiaromaticity through their effect on the tilt angle between the substituents and the isophlorin macrocycle.

The antiaromatic character of S_2O_2Iphs decreased in the order **1e** > **1d** > **1a** > **1b** > **1c**, directly correlating with the structural changes driven by the substituent bulk. Unsubstituted (**1e**) and orthogonally substituted (**1d**) isophlorins maintained completely planar macrocycles with strong antiaromaticity. As the tilt angle decreased from **1a** to **1c** due to decreasing steric hindrance, the extent of π-conjugation between the substituents and the macrocycle increased, leading to weaker antiaromaticity. Our findings highlight the dual requirements for stable antiaromatic systems: electron-withdrawing groups are

necessary to lower the HOMO energies and prevent oxidation, whereas their steric bulk influences the degree of antiaromaticity preservation.

This research provides a clear structure–property relationship that guides the rational design of functional antiaromatic materials with tunable electronic properties. Although we were unable to isolate the sterically demanding 2,6-dichlorophenyl derivative (**1d**) which combines strong antiaromaticity with sufficient stability, our results revealed strategies for balancing these competing properties. These insights contribute to the growing field of antiaromatic material design for potential applications in organic electronics and optoelectronic devices. Future work will focus on developing isophlorin derivatives that maintain strong antiaromaticity through appropriate substituent orientation while achieving sufficient stability through electron-withdrawing effects without compromising macrocycle planarity.

4. Experimental Section

4.1. Instrumentation and Materials

S_2O_2Iph **1a** was synthesized by the previously reported procedure.[20] All other chemicals were of reagent grade and used without further purification unless otherwise noted. Analytical thin-layer chromatography (TLC) was performed on silica gel 60 F_{254} plates (Merck). Column chromatography was performed using silica gel 60N (Kanto Chemical, spherical, neutral, 63–210 μm). All NMR spectral data were recorded on a JEOL ECA-500 (500 MHz), JEOL ECS-400 (400 MHz), and Bruker AVANCE NEO (700 MHz) spectrometers at ambient temperature (25 °C). ^{1}H NMR spectra were referenced internally to tetramethylsilane as a standard. ^{13}C NMR spectra were referenced internally to a solvent signal (δ = 77.0 and 29.8 ppm for $CDCl_3$ and [D_6]acetone, respectively). High-resolution electrospray ionization mass spectrometry (ESI HRMS) data were obtained using a Thermo Fisher Scientific Q-Exactive mass spectrometer. MALDI-TOF MS data were obtained using a SHIMADZU KRATOS AXIMA-PERFORMANCE mass spectrometer. UV/vis spectral data were recorded on a HITACHI U-4100 spectrometer. Melting points were determined using a Yanaco MP-S3 melting point apparatus.

4.2. Synthesis of 2,5-bis-((3,5-bis-(trifluoromethyl)phenyl)hydroxymethyl)thiophene (2b)

Under N_2 atmosphere, *n*-BuLi (2.6 M solution in hexane, 20 mL, 53 mmol) and *N,N,N′,N′*-tetramethylethylenediamine (8 mL, 53.7 mmol) was added in dry hexane (50 mL) and stirred for 10 min at room temperature. To the resultant solution was added thiophene (1.7 mL, 21 mmol), and stirred at 50 °C for 1 hour. The resultant light-yellow suspended solution was cooled to 0 °C, and then added dropwise 3,5-bis(trifluoromethyl)benzaldehyde (8.7 mL, 52.8 mmol) in THF (48 mL). The resultant solution was stirred for 20 min, and the quenched by saturated aq. NH_4Cl. The product was extracted with EtOAc, and then the organic layer was washed with water and brine, and then dried over Na_2SO_4. Solvent was removed under the reduced pressure. The crude product was purified by recrystallization from EtOAc/hexane to give the title compound as pale brown solid (6.0 g, 10.8 mmol, 50%) The NMR analysis suggested that **2b** was obtained as a mixture of diastereomers. ^{1}H NMR (500 MHz, $CDCl_3$) δ = 7.90 (s, 4H), 7.83 (s, 2H), 6.82 (s, 2H), 6.12 (s, 2H), 2.61 ppm (brs, 2H); ^{13}C NMR (125 MHz, [D_6]acetone) δ = 149.4 (Cq), 149.1 (Cq), 148.9 (Cq), 148.9 (Cq), 132.0 (q, J = 33 Hz, Cq), 127.5 (CH), 125.40 (CH), 125.38 (CH), 124.5 (q, J = 270 Hz, CF_3), 121.9 (CH), 71.1 ppm (*C*H); elemental analysis calcd (%) for $C_{22}H_{12}F_{12}O_2S$: C 46.49, H 2.13, N 0; found: C, 46.71, H 2.13, N 0.

4.3. Synthesis of 2,5-bis-((5-cyanothien-2-yl)hydroxymethyl)thiophene (2c)

Under N_2 atmosphere, *n*-BuLi (2.67 M solution in hexane, 2.9 mL, 7.5 mmol) and *N,N,N′,N′*-tetramethylethylenediamine (1.1 mL, 7.5 mmol) was added in dry hexane (7.5 mL) and stirred for 10 min at room temperature. To the resultant solution was added thiophene (0.27 mL, 3.4 mmol), and stirred at 50 °C for 1 hour. The resultant light-yellow suspended solution was cooled to 0 °C, and then added dropwise 5-formylthiophene-2-carbonitrile (0.929 mg, 6.7 mmol) in THF (7.5 mL). The resultant solution was stirred for 15 min at 0 °C, and then 1 hour at room temperature. The resultant solution was quenched by saturated aq. NH_4Cl. The product was extracted with EtOAc, and then the organic layer was washed with water (× 1) and brine (× 1), and then dried over Na_2SO_4. Solvent was removed under the reduced pressure. The crude product was purified by column chromatography (silica gel, hexane/EtOAc 1:1). A fraction containing the desired product was concentrated under vacuum to give the title compound as yellow oil (642.9 mg, 1.90 mmol, 53%). The NMR analysis suggested that **2c** was obtained as a mixture of diastereomers. R_f = 0.20 (hexane/EtOAc 1:1); ^{1}H NMR (500 MHz, $CDCl_3$) δ = 7.90 (s, 4H), 7.83 (s, 2H), 6.82 (s, 2H), 6.12 (s, 2H), 1.61 ppm (brs, 2H); ^{13}C NMR (125 MHz, $CDCl_3$) δ = 155.2 (*C*q), 155.1 (*C*q), 146.7 (*C*q), 146.6 (*C*q), 137.5 (*C*H), 125.3 (*C*H), 125.2 (*C*H), 124.89 (*C*H), 124.85 (*C*H), 114.2 (*C*q), 109.1 (*C*q), 77.3 (*C*q), 77.0 (*C*q), 76.7 (*C*q), 68.3 (*C*H), 68.2 ppm (*C*H); HRMS(ESI): *m/z* calcd for $C_{16}H_9N_2O_2S_3$: 356.9832 ([M − H]$^-$), found 356.9834.

4.4. Synthesis of 2,5-bis-((5-cyanothien-2-yl)-(fur-2-yl)methyl)thiophene (3c)

To a solution of **2c** (555 mg, 1.55 mmol) and freshly distilled furan (0.44 mL, 6.0 mmol) in dry dichloromethane (150 mL), BF_3·OEt_2 (25 μL, 0.25 mmol) was added. The resultant solution was stirred at room temperature under N_2 for 2 hours. The resultant solution was washed with saturated aq. $NaHCO_3$ (× 1), water (× 1), and brine (× 1), and then dried over Na_2SO_4. Solvent was removed under the reduced pressure to give the title compound as brown oil (358 mg, 0.295 mmol, 50%). The NMR analysis suggested that **3c** was obtained as a mixture of diastereomers. R_f = 0.54 ($CHCl_3$); ^{1}H NMR (500 MHz, $CDCl_3$) δ = 7.47 (d, J = 3.8 Hz, 2H), 7.42–7.38 (m, 2H), 6.90 (d, J = 3.8 Hz, 2H), 6.77 (d-like, 2H), 6.36 (dd, J = 3.2, 1.9 Hz, 2H), 6.20 (d, J = 3.2 Hz, 2H), 5.82 ppm (s, 2H); ^{13}C NMR (125 MHz, $CDCl_3$) δ = 153.0 (*C*q), 152.7 (*C*q), 142.9 (*C*q), 142.8 (*C*q1), 137.4 (*C*H), 126.3 (*C*H), 126.1 (*C*H), 114.1 (*C*q), 110.5 (*C*H), 109.2 (*C*H), 108.2 (*C*H), 41.4 ppm (*C*H); HRMS(ESI): *m/z* calcd for $C_{24}H_{13}N_2O_2S_3$: 457.0145 ([M − H]$^-$), found 457.0137.

4.5. Synthesis of 5,10,15,20-tetrakis(3,5-bis-(trifluoromethyl)phenyl)-21,23-dioxa-22,24-dithiaisophlorin (1b)

To a solution of **2b** (563 mg, 1.00 mmol) and freshly distilled furan (0.080 mL, 1.0 mmol) in dry dichloromethane (200 mL), BF_3·OEt_2 (0.25 mL, 1.0 mmol) was added. The resultant solution was stirred at room temperature under N_2 for 2 hours. The resultant solution was added $FeCl_3$ (1644 mg, 10 mmol), and then stirred for 30 min. The resultant solution was washed with water (× 3). The organic layer was

poured on top of a basic alumina column packed with CH_2Cl_2, then eluted with CH_2Cl_2. The obtained product was further purified by column chromatography (silica gel, hexane/CH_2Cl_2 10:1). A fraction containing the desired product was concentrated under vacuum, and the obtained green powder was washed with hexane, and then recrystallized from hot acetonitrile to give the title compound as green needle microcrystals (45 mg, 0.037 mmol, 7%). M.p.: >300 °C; ^{1}H NMR (400 MHz, $CDCl_3$) δ = 7.49 (s, 4H), 6.96 (s, 8H), 3.37 (s, 4H), 3.35 ppm (s, 4H); ^{13}C NMR (175 MHz, $CDCl_3$) δ = 147.3 (*Cq*), 136.3 (*Cq*), 132.8 (q, J = 32 Hz, *Cq*), 129.0 (*CH*), 128.8 (*CH*), 127.9 (*CH*), 124.8 (*Cq*), 122.6 (q, J = 270 Hz, CF_3), 122.1 (*CH*), 113.8 (*Cq*); UV/Vis (CH_2Cl_2): λ_{max} (Logε) = 342 (4.87), 381 (4.88), 441 (3.82), 472 (3.71), 506 (3.41), 780 nm (br, 2.72); HRMS(ESI): *m/z*: calcd for $C_{52}H_{20}F_{24}O_2S_2$: 1196.0516 ($[M]^+$); found: 1196.0517, elemental analysis calcd (%) for $C_{52}H_{20}F_{24}O_2S_2$: C, 52.19; H, 1.68; N, 0; found: C, 52.10; H, 1.67; N, 0.

4.6. Synthesis of 5,10,15,20-tetrakis(5-cyanothien-2-yl)-21,23-dioxa-22,24-dithiaisophlorin (1c)

To a solution of **2c** (404 mg, 1.13 mmol) and **3c** (304 mg, 0.66 mmol) in dry dichloromethane (200 mL), BF_3·OEt_2 (0.015 mL, 1.1 mmol) was added. The resultant solution was stirred at room temperature under N_2 for 2 hours. The resultant solution was added DDQ (439 mg, 1.95 mmol), and then stirred for 30 min. The resultant solution was poured on top of a basic alumina column packed with CH_2Cl_2, then eluted with CH_2Cl_2. The obtained crude powder product was washed with acetonitrile, and then hexane to give the title compound as dark green powder (54 mg, 0.0069 mmol, 8.9%). R_f = 0.24 (CH_2Cl_2); m.p.: >300 °C; ^{1}H NMR (400 MHz, $CDCl_3$) δ = 7.18 (d, J = 3.7 Hz, 4H), 6.33 (d, J = 3.9 Hz, 4H), 4.25 (s, 4H), 4.15 ppm (s, 4H); ^{13}C NMR spectrum was not obtained because of low solubility of the compounds; UV/vis (CH_2Cl_2): λ_{max} (Relative Intensity) = 348 (1.13), 399 (1), 520 (sh, 0.08), 715 nm (br, 0.01); HRMS(ESI): *m/z*: calcd for $C_{40}H_{16}N_4O_2S_6$: 775.9603 ($[M]^-$); found: 775.9607.

4.7. DFT Calculations

All calculations were carried out using the Gaussian 16 program package (Revision C.01).[53] Geometries of all models were optimized by the DFT method at the cam-B3LYP/6-311G(d,p) level in the gas phase. To confirm that the optimized geometries were not in the saddle but stable points, frequency calculations were performed.

Nucleus-independent chemical shifts (NICS) values were calculated at the GIAO-cam-B3LYP/6-311+G(2d,p) level using geometry-optimized structures. Magnetically induced current densities were calculated using the GIMIC program[41,42] based on the optimized structure. The NMR shielding constants were calculated using gauge-including atomic orbitals (GIAO) at cam-B3LYP/6-311+G(2d,p) level. The integration of the current density through a bond (nA T^{-1}) was performed using a rectangular plane perpendicular to the plane of the macrocycle. The rectangular plane had dimensions of 10 bohr (5.2 Å) high 4.4 bohr (2.3 Å) wide and spanned the center of the bond of interest. The magnetic field was placed perpendicular to the plane of the macrocycle. Electronic indices of aromaticity (AV1245[48] and AV_{min}[49,50]) were calculated with the AIMAll[54] and ESI-3D[55,56] program packages.

Acknowledgements

This work was supported by JSPS KAKENHI Grant Numbers JP17K14447, JP19H02688, and Iketani Science and Technology Foundation (No. 0361035-A). H. S. is grateful for a JSPS Research Fellow (24KJ1558). We thank Dr. Yosuke Tani (The University of Osaka) and Prof. Dr. Takuji Ogawa (The University of Osaka) for helpful discussion. We also thank Prof. Dr. Shohei Saito (The University of Osaka) and Dr. Kensuke Suga (Kyoto University) for helping with ESi-3D and AIMAll program. Measurements were performed at the Analytical Instrument Facility, Graduate School of Science, Osaka University. The computation was performed using Research Center for Computational Science, Okazaki, Japan (Projects: 21-IMS-C218, 22-IMS-C217, and 23-IMS-C224).

Conflict of Interests

The authors declare no conflict of interest.

Data Availability Statement

The data that support the findings of this study are available in the supporting information of this article.

Keywords: Antiaromaticity · Computational Chemistry · Isophlorin · Porphyrinoids · Substituent Effects

[1] R. Breslow, *Acc. Chem. Res.* **1973**, *6*, 393–398.
[2] R. Gleiter, G. Haberhauer, *Aromaticity and Other Conjugation Effects*, Wiley-VCH Verlag, Weinheim, Germany, **2012**.
[3] Ed. (I. Fernandez), *Aromaticity: Modern Computational Methods and Applications*, Elsevier Science Publishing, Philadelphia, PA, **2021**.
[4] J.-Y. Shin, T. Yamada, H. Yoshikawa, K. Awaga, H. Shinokubo, *Angew. Chem., Int. Ed.* **2014**, *53*, 3096–3101.
[5] S. Fujii, S. Marqués-González, J. Y. Shin, H. Shinokubo, T. Masuda, T. Nishino, N. P. Arasu, H. Vázquez, M. Kiguchi, *Nat. Commun.* **2017**, *8*, 4–11.
[6] T. Stuyver, M. Perrin, P. Geerlings, F. De Proft, M. Alonso, *J. Am. Chem. Soc.* **2018**, *140*, 1313–1326.
[7] C. Hong, J. Baltazar, J. D. Tovar, *Eur. J. Org. Chem.* **2022**, *2022*, e202101343.
[8] J. Wu, Y. Chen, J. Liu, Z. Pang, G. Li, Z. Lu, Y. Huang, A. Facchetti, T. J. Marks, *J. Mater. Chem. C* **2022**, *10*, 2724–2731.
[9] X.-L. Zheng, H.-S. Lin, B.-W. Zhang, S. Maruyama, Y. Matsuo, *J. Org. Chem.* **2022**, *87*, 5457–5463.
[10] R. Santiago, M. À. Carvajal, J. Poater, I. de P. R. Moreira, S. T. Bromley, M. Deumal, J. Ribas-Ariño, *Chem. Sci.* **2024**, *16*, 430–447.
[11] J. Sprachmann, T. Wachsmuth, M. Bhosale, D. Burmeister, G. J. Smales, M. Schmidt, Z. Kochovski, N. Grabicki, R. Wessling, E. J. W. List-Kratochvil, B. Esser, O. Dumele, *J. Am. Chem. Soc.* **2023**, *145*, 2840–2851.
[12] W. E. Meador, M. A. Saucier, M. R. Tucker, N. A. Kruse, A. J. Mobley, C. R. Brower, S. R. Parkin, K. M. Clark, N. I. Hammer, G. S. Tschumper, J. H. Delcamp, *Chem. Sci.* **2024**, *15*, 12349–12360.
[13] R. Lavendomme, M. Yamashina, *Chem. Sci.* **2024**, *15*, 18677–18697.
[14] J. L. Sessler, D. Seidel, *Angew. Chem., Int. Ed.* **2003**, *42*, 5134–5175.
[15] S. Saito, A. Osuka, *Angew. Chem., Int. Ed.* **2011**, *50*, 4342–4373.
[16] A. Osuka, S. Saito, *Chem. Commun.* **2011**, *47*, 4330–4339.
[17] B. K. Reddy, A. Basavarajappa, M. D. Ambhore, V. G. Anand, *Chem. Rev.* **2017**, *117*, 3420–3443.
[18] P. Pushpanandan, M. Ravikanth, *Chem. Rec.* **2022**, *22*, e202200144.
[19] R. Bachmann, F. Gerson, G. Gescheidt, E. Vogel, *J. Am. Chem. Soc.* **1992**, *114*, 10855–10860.
[20] J. S. Reddy, V. G. Anand, *J. Am. Chem. Soc.* **2008**, *130*, 3718–3719.
[21] T. Ito, Y. Hayashi, S. Shimizu, J.-Y. Shin, N. Kobayashi, H. Shinokubo, *Angew. Chem., Int. Ed.* **2012**, *51*, 8542–8545.
[22] R. Nozawa, K. Yamamoto, J.-Y. Shin, S. Hiroto, H. Shinokubo, *Angew. Chem., Int. Ed.* **2015**, *54*, 8454–8457.
[23] T. Yoshida, D. Sakamaki, S. Seki, H. Shinokubo, *Chem. Commun.* **2017**, *53*, 1112–1115.

[24] S.-Y. Liu, H. Tanaka, R. Nozawa, N. Fukui, H. Shinokubo, *Chem. - Eur. J.* **2019**, *25*, 7618–7622.
[25] S. Ukai, Y. H. Koo, N. Fukui, S. Seki, H. Shinokubo, *Dalton Trans.* **2020**, *49*, 14383–14387.
[26] S. Ukai, A. Takamatsu, M. Nobuoka, Y. Tsutsui, N. Fukui, S. Ogi, S. Seki, S. Yamaguchi, H. Shinokubo, *Angew. Chem., Int. Ed.* **2022**, *61*, e202114230.
[27] S. Itabuchi, R. Nozawa, T. Yoshida, N. Fukui, H. Shinokubo, *J. Porphyrins Phthalocyanines* **2023**, *27*, 121–125.
[28] S. Kino, S. Ukai, N. Fukui, R. Haruki, R. Kumai, Q. Wang, S. Horike, Q. M. Phung, D. Sundholm, H. Shinokubo, *J. Am. Chem. Soc.* **2024**, *146*, 9311–9317.
[29] S.-Y. Liu, S. Li, S. Ukai, R. Nozawa, N. Fukui, R. Sugimori, R. Kishi, H. Shinokubo, *Chem. - Eur. J.* **2024**, *30*, e202400292.
[30] S. Ishikawa, K. Yamasumi, S. Sugiura, S. Sato, G. Watanabe, Y. H. Koo, S. Seki, Y. Bando, Y. Haketa, H. Shinokubo, H. Maeda, *Chem. Sci.* **2024**, *15*, 7603–7609.
[31] M. Takase, T. Takata, K. Oki, S. Mori, H. Uno, *Chem. Sci.* **2023**, *14*, 7036–7043.
[32] R. F. Salikov, A. Y. Belyy, M. K. Ilyushchenko, D. N. Platonov, A. D. Sokolova, Y. V. Tomilov, *Chem. - Eur. J.* **2024**, *30*, e202401041.
[33] Y. Tanaka, T. Tsutsumi, S. Mori, Y. Ide, T. Ikeue, S. Shimizu, *Chem. Asian J.* **2025**, *20*, e202401337.
[34] K. Yamashita, K. Nakajima, Y. Honda, T. Ogawa, *Chem. - Eur. J.* **2020**, *26*, 3633–3640.
[35] H. Sugimura, K. Nakajima, K. Yamashita, T. Ogawa, *Eur. J. Org. Chem.* **2022**, e202200747.
[36] J. S. Reddy, V. G. Anand, *J. Am. Chem. Soc.* **2009**, *131*, 15433–15439.
[37] R. R. Valiev, H. Fliegl, D. Sundholm, *J. Phys. Chem. A* **2013**, *117*, 9062–9068.
[38] F. Feixas, E. Matito, J. Poater, M. Solà, *Chem. Soc. Rev.* **2015**, *44*, 6434–6451.
[39] P. V. R. Schleyer, C. Maerker, A. Dransfeld, H. Jiao, N. J. R. van Eikema Hommes, *J. Am. Chem. Soc.* **1996**, *118*, 6317–6318.
[40] C. Corminboeuf, P. von R. Schleyer, R. Puchta, C. S. Wannere, Z. Chen, *Chem. Rev.* **2005**, *105*, 3842–3888.
[41] J. Jusélius, D. Sundholm, J. Gauss, *J. Chem. Phys.* **2004**, *121*, 3952–3963.
[42] D. Sundholm, H. Fliegl, R. J. F. Berger, *WileyInterdiscip. Rev. Comput. Mol. Sci.* **2016**, *6*, 639–678.
[43] R. R. Valiev, H. Fliegl, D. Sundholm, *Phys. Chem. Chem. Phys.* **2017**, *19*, 25979–25988.
[44] J. Kruszewski, T. M. Krygowski, *Tetrahedron Lett.* **1972**, *13*, 3839–3842.
[45] T. M. Krygowski, H. Szatylowicz, O. A. Stasyuk, J. Dominikowska, M. Palusiak, *Chem. Rev.* **2014**, *114*, 6383–6422.
[46] E. M. Arpa, S. Stafström, B. Durbeej, *J. Org. Chem.* **2025**, *90*, 1297–1308.
[47] H. L. Schmider, A. D. Becke, *Theochem* **2000**, *527*, 51–61.
[48] E. Matito, *Phys. Chem. Chem. Phys.* **2016**, *18*, 11839–11846.
[49] C. García-Fernández, E. Sierda, M. Abadía, B. Bugenhagen, M. H. Prosenc, R. Wiesendanger, M. Bazarnik, J. E. Ortega, J. Brede, E. Matito, A. Arnau, *J. Phys. Chem. C* **2017**, *121*, 27118–27125.
[50] I. Casademont-Reig, T. Woller, J. Contreras-García, M. Alonso, M. Torrent-Sucarrat, E. Matito, *Phys. Chem. Chem. Phys.* **2018**, *20*, 2787–2796.
[51] I. Casademont-Reig, T. Woller, V. García, J. Contreras-García, W. Tiznado, M. Torrent-Sucarrat, E. Matito, M. Alonso, *Chem. - Eur. J.* **2023**, *29*, e202202264.
[52] E. Desmedt, I. Casademont-Reig, R. Monreal-Corona, F. De Vleeschouwer, M. Alonso, *Chem. - Eur. J.* **2024**, *30*, e202401933.
[53] M. J. Frisch, G. W. Trucks, H. B. Schlegel, G. E. Scuseria, M. A. Robb, J. R. Cheeseman, G. Scalmani, V. Barone, G. A. Petersson, H. Nakatsuji, X. Li, M. Caricato, A. V. Marenich, J. Bloino, B. G. Janesko, R. Gomperts, B. Mennucci, H. P. Hratchian, J. V. Ortiz, A. F. Izmaylov, J. L. Sonnenberg, D. Williams-Young, F. Ding, F. Lipparini, F. Egidi, J. Goings, B. Peng, A. Petrone, T. Henderson, D. Ranasinghe, V. G. Zakrzewski, J. Gao, N. Rega, G. Zheng, W. Liang, M. Hada, M. Ehara, K. Toyota, R. Fukuda, J. Hasegawa, M. Ishida, T. Nakajima, Y. Honda, O. Kitao, H. Nakai, T. Vreven, K. Throssell, J. A. Montgomery Jr, J. E. Peralta, F. Ogliaro, M. J. Bearpark, J. J. Heyd, E. N. Brothers, K. N. Kudin, V. N. Staroverov, T. A. Keith, R. Kobayashi, J. Normand, K. Raghavachari, A. P. Rendell, J. C. Burant, S. S. Iyengar, J. Tomasi, M. Cossi, J. M. Millam, M. Klene, C. Adamo, R. Cammi, J. W. Ochterski, R. L. Martin, K. Morokuma, O. Farkas, J. B. Foresman, D. J. Fox, Gaussian, Inc., Gaussian16, Revision C.01, **2016**.
[54] T. A. Keith, AIMAll (Version 19.10.12), TK Gristmill Software, Overland Park KS, USA, **2019**.
[55] E. Matito, M. Solà, P. Salvador, M. Duran, *Faraday Discuss.* **2007**, *135*, 325–345.
[56] E. Matito, ESi-3D: Electron Sharing Indexes Program for 3D Molecular Space Partitioning, Institute Of Computational Chemistry And Catalysis, University Of Girona, Catalonia, Spain, **2015**.

Manuscript received: March 25, 2025
Revised manuscript received: May 2, 2025
Version of record online: ■■, ■■